Estimating the Effective Radiative Forcing of Contrail Cirrus

MARIUS BICKEL, MICHAEL PONATER, LISA BOCK, ULRIKE BURKHARDT, AND SVENJA REINEKE

Deutsches Zentrum für Luft- und Raumfahrt, Institut für Physik der Atmosphäre, Oberpaffenhofen, Germany

(Manuscript received 26 June 2019, in final form 24 October 2019)

ABSTRACT

Evidence from previous climate model simulations has suggested a potentially low efficacy of contrails to force global mean surface temperature changes. In this paper, a climate model with a state-of-the-art contrail cirrus representation is used for fixed sea surface temperature simulations in order to determine the effective radiative forcing (ERF) from contrail cirrus. ERF is expected to be a good metric for intercomparing the quantitative importance of different contributions to surface temperature and climate impact. Substantial upscaling of aviation density is necessary to ensure statistically significant results from our simulations. The contrail cirrus ERF is found to be less than 50% of the respective instantaneous or stratosphere adjusted radiative forcings, with a best estimate of roughly 35%. The reduction of ERF is much more substantial for contrail cirrus than it is for a CO_2 increase when both stratosphere adjusted forcings are of similar magnitude. Analysis of all rapid radiative adjustments contributing to the ERF indicates that the reduction is mainly induced by a compensating effect of natural clouds that provide a negative feedback. Compared to the CO_2 reference case, a less positive combined water vapor and lapse rate adjustment also contributes to a more distinct reduction of contrail cirrus ERF, but not as much as the natural cloud adjustment. Based on the experience gained in this paper, respective contrail cirrus simulations with interactive ocean will be performed as the next step toward establishing contrail cirrus efficacy. ERF results of contrail cirrus from other climate models equipped with suitable parameterizations are regarded as highly desirable.

1. Introduction

The global climate impact from aviation has been repeatedly reviewed over the last 20 years (e.g., Penner et al. 1999; Sausen et al. 2005; Lee et al. 2009, 2010; Brasseur et al. 2016). Its contribution to anthropogenic climate change is currently assessed as ranging between 4% and 5% (Lee et al. 2010; Kärcher 2018), while extra attention has also been motivated by high aviation growth rates expected for the years to come (e.g., Schäfer and Waitz 2014; Brasseur et al. 2016). CO_2 emissions from fuel burning and several non-CO_2 effects contribute to the total radiative forcing of aviation with comparable magnitude. Indirect climate effects of aircraft aerosol emissions are potentially large (e.g., Gettelman and Chen 2013; Zhou and Penner 2014; Righi et al. 2016; Penner et al. 2018) but have remained highly uncertain due to open issues in our knowledge of aerosol–cloud interactions (Kärcher 2017; Kärcher 2018). In contrast, the level of understanding for contrail cirrus impact has been thoroughly upgraded during the last 10 years, and it is currently considered as the largest component contributing to aircraft-induced radiative forcing (Burkhardt and Kärcher 2011; Schumann and Graf 2013; Bock and Burkhardt 2016b; Grewe et al. 2017).

Due to its close link to global mean surface temperature change via the so-called climate sensitivity parameter, radiative forcing has been the established metric base for assessing the relevance of contributors to global climate change for some decades (National Research Council 2005; Ramaswamy et al. 2019). A correct assessment of such individual contributions is particularly required, if one component effect is to be mitigated at the expense of another. For example, contrail effects may be avoided by flying beneath or around areas susceptible for contrail formation and persistence (e.g., Mannstein et al. 2005; Chen et al. 2012; Dahlmann et al. 2016; Grewe et al. 2017), accepting a slightly higher fuel consumption in the process. However, some previous studies dealing with the surface temperature impact of line-shaped contrails have cast doubt on the degree of reliability that radiative forcing has for such assessments. Using a climate model equipped with a parameterization for

Denotes content that is immediately available upon publication as open access.

Corresponding author: Marius Bickel, marius.bickel@dlr.de

DOI: 10.1175/JCLI-D-19-0467.1

line-shaped contrails and a mixed layer ocean as lower boundary, Ponater et al. (2005) and Ponater (2010) found that contrail radiative forcing has an efficacy of about 0.6, meaning that the contrail climate sensitivity (i.e., the global mean surface temperature response per unit radiative forcing) was only 60% of the climate sensitivity to a CO_2 forcing of comparable magnitude. With a similar model setup (but a considerably different parameterization for line-shaped contrails), Rap et al. (2010) calculated an even lower efficacy value (0.31). Ramaswamy et al. (2019) rightly point out that neither study could establish a convincing physical reason for the reduced efficacy of line-shaped contrails. As for the more relevant contrail cirrus (i.e., for aviation-induced cirrus without specifically linear structure), no efficacy estimate is currently available at all.

The evidence of differing efficacies for different forcings is not limited to aviation effects but has been established in a more generic way, particularly for nonhomogeneous radiative perturbations to the climate system (e.g., Joshi et al. 2003; Hansen et al. 2005; Berntsen et al. 2005; Shindell 2014). To cope with the resulting conceptual problems, alternatives to the classical definition of the "stratosphere adjusted radiative forcing" (RF_{adj}) (Manabe and Wetherald 1967; Forster et al. 1997; Hansen et al. 1997) have been developed. The concept of "effective radiative forcing" (ERF) (e.g., Myhre et al. 2013), which includes in the radiative forcing value all feedback-like radiative adjustments occurring on short time scales, is now assessed to ensure a much smaller variation of different forcing efficacies around the reference case of CO_2 increase (e.g., Lohmann et al. 2010; Shine et al. 2012; Sherwood et al. 2015; Marvel et al. 2016). It has therefore been adopted as the definition of choice in the IPCC Fifth Assessment Report (AR5; IPCC 2013), with Figs. 8.15 and 8.17 within that volume being exemplary for the quantitative comparison of individual climate change forcers in terms of ERF.

It is important to note that the AR5 asserts giving an ERF estimate of contrail cirrus (Boucher et al. 2013) but in fact it does not, as acknowledged in the supplement to the respective chapter 7: The original work fundamental to the AR5 estimate (Myhre et al. 2013, their Table 8.6) had no intention of following the methodologies suitable to calculate ERF (Hansen et al. 2005; Forster et al. 2016). Only in Burkhardt and Kärcher (2011) has one rapid radiative adjustment (from natural clouds) induced by the presence of contrail cirrus been determined, which reduces their RF_{adj} estimate for 2002 from 39 to 31 mW m^{-2}. A later study (Chen and Gettelman 2013) reports a considerably lower contrail cirrus radiative forcing estimate of 13 mW m^{-2} for 2006. Its simulation concept comes nearer to the ERF methodology but was used in a variant (specified dynamics simulations) that Forster et al. (2016) assume as unlikely to give a full account of rapid radiative adjustments. An evaluative comparison of the various estimates is difficult, however, because the methodological approaches differ in many ways, including the parameterization of contrail cirrus and the flight inventories involved.

In the present study, we will present the first clear-cut calculation of contrail cirrus ERF using the method of fixed sea surface temperature radiative forcing (e.g., Shine et al. 2003; Hansen et al. 2005), which is one of the approved practical realizations of the ERF concept (Forster et al. 2016). Our approach fundamentally relies on a recently developed advanced contrail parameterization in a state-of-the-art climate model (Bock and Burkhardt 2016a). We will address potential physical reasons for an unusually strong reduction of contrail cirrus ERF, compared to the conventional RF_{adj}, through a comprehensive analysis of rapid radiative adjustments, by and large following the methodical concept applied in Vial et al. (2013). Hence, in section 2 we will describe and motivate the model setup and the way in which the simulations and the model data analysis were conducted. Section 3 will present the results, while in sections 4 and 5 these results will be discussed in the context of current knowledge and conclusions will be drawn, together with suggestions for further work on the contrail cirrus efficacy issue.

2. Model, simulations, and analysis methods

a. *Model and parameterization*

The ECHAM climate model (i.e., ECWMF model, Hamburg version) reviewed by Stevens et al. (2013) has a long established history for use in numerous fields of Earth system science (e.g., Giorgetta et al. 2006), and also as a suitable framework for contrail global climate impact studies (e.g., Marquart et al. 2003; Ponater et al. 2005; Burkhardt and Kärcher 2009). Here, it is adopted in its fifth-generation version, ECHAM5 (Roeckner et al. 2004, 2006), which has been equipped with a microphysical two-moment contrail cirrus parameterization (CCMod) (Bock and Burkhardt 2016a). Contrail cirrus in ECHAM5-CCMod is described by its coverage, its volume and length, and its ice water mixing ratio and ice crystal number concentration as prognostic variables. The description of contrail cirrus builds on the two-moment scheme for natural ice clouds in ECHAM5 (Lohmann et al. 2008), with a number of modifications and extensions described by Bock and Burkhardt (2016a). Aviation-induced cirrus is consistently embedded in the hydrological cycle, meaning that contrail cirrus and natural cirrus compete for water vapor available for condensation (Burkhardt and Kärcher 2009). Parameterized processes include

contrail formation, volume growth due to turbulent diffusion and sedimentation, spreading from wind shear, deposition, and loss of ice crystals from sublimation, sedimentation, and precipitation. Details are explained in Bock and Burkhardt (2016a,b), where the model has also been evaluated against observations. In particular, accounting for ice crystal number concentration in the two-moment scheme helps to overcome a substantial low optical depth bias that has been identified in previous ECHAM contrail parameterizations (Kärcher et al. 2010), although many methodical differences make an exact comparison between optical properties derived from global model simulations and satellite (let alone in situ) observations an intricate task (Kärcher et al. 2009; Minnis et al. 2013). We note that the ECHAM5 model version used here has a cold bias, larger in the extratropics than in the tropics. However, the resulting overestimation of contrail formation is stronger at tropical latitudes, where the number of situations close to the threshold temperature of contrail formation is larger (Bier and Burkhardt 2019).

The main purpose of ECHAM5-CCMod is the determination of contrail-cirrus radiative forcing and climate impact. The stratosphere adjusted radiative forcing (RF_{adj}) is calculated online by radiation double calling (Stuber et al. 2001). In a benchmark test setup with 1% additional cirrus of optical depth 0.3, globally at 200 hPa (Myhre et al. 2009), the ECHAM5 radiation parameterization yields an RF_{adj} value of 113 mW m^{-2} (Dietmüller et al. 2016). The latter paper also reports (for contrails) a small difference between RF_{adj} and the instantaneous radiative forcing (RF_{inst}) that has usually been given in other contrail studies. Premising that, contrail radiative forcing from ECHAM5 is found to lie within the range spanned by other radiation modules (Myhre et al. 2009; Schumann et al. 2012).

Bock and Burkhardt (2016b, 2019) have used ECHAM5-CCMod to determine RF_{adj}, using aircraft inventories from the Aviation Environmental Design Tool (AEDT) (Wilkerson et al. 2010; FESG 1998) for describing air traffic density in their simulations. Estimates of 49 mW m^{-2} are given for 2006 and 160 mW m^{-2} for 2050. The 2006 estimate is similar to most other values given for years near 2005 (Burkhardt and Kärcher 2011; Schumann and Graf 2013; Schumann et al. 2015). However, ECHAM5-CCMod estimates considerably exceed those yielded within the CAM5 climate model framework (see Chen and Gettelman 2016, their Fig. 3a). The AEDT inventory for 2050 will also be used for the present study.

b. *The simulation concept*

From the various radiative forcing definitions established in climate research (Hansen et al. 2005; Myhre et al. 2013) we address within this study RF_{inst}, RF_{adj}, and ERF, which are determined by specially designed types of climate model simulations. Both RF_{inst} and RF_{adj} are calculated from a single simulation with a pair of radiative transfer calls—one with and one without perturbation (here either contrails or CO_2) at each time step. Due to very small statistical uncertainties a simulation length of 5 years is sufficient to obtain a robust RF_{inst}. No adjustments of the atmosphere to the perturbation are allowed in the RF_{inst} calculation. RF_{adj} is determined in the same way as RF_{inst} by a single simulation with two radiative transfer calculations, but using the method described by Stuber et al. (2001), where temperature in the stratosphere of the perturbed radiative transfer calculation is allowed to adjust to new equilibrium. Tropospheric temperature remains fixed. An integration length of 5 years is still sufficient. RF_{adj} for a long time has been considered a solid basis for intercomparing the expected climate impact of various perturbations and has been used in previous radiative forcing estimates with ECHAM (Marquart et al. 2003; Ponater et al. 2006; Burkhardt and Kärcher 2011; Bock and Burkhardt 2016b).

ERF is calculated following the fixed sea surface temperature (FSST) method as recommended by Forster et al. (2016). In an ideal methodical approach surface temperature would be fixed everywhere in order to separate slow feedbacks (developing with ocean temperature change) from rapid adjustments (driven by atmospheric changes directly induced by the forcing perturbation). However, prescribing land surface temperatures often cause technical problems in climate models (e.g., Hansen et al. 2005), so it is an approved alternative to fix the sea surface temperature only. Experience has shown that global mean surface temperature cannot change substantially anyway when sea surface temperatures are fixed. Some papers even consider the interactive land surface temperatures as conceptually desirable, representing another rapid temperature adjustment at relatively short time scales compared to ocean temperatures (e.g., Vial et al. 2013; Smith et al. 2018). Technically, ERF is determined as the TOA net radiative flux difference between two independent FSST simulations, one with perturbation (experiment) and one without (reference). In contrast to methods determining ERF from regression (Gregory et al. 2004), the statistical uncertainties of the FSST method are substantially lower with the same number of simulation years (Forster et al. 2016). Nevertheless the statistical uncertainties of ERF are larger than for RF_{inst} and RF_{adj} and thus a larger integration length of at least 25 years is required to get significant results, even for forcings with a magnitude around 1 W m^{-2}. Hence, it has been common to determine ERF from simulations with larger forcings like CO_2 doubling (Forster et al. 2016; Smith et al. 2018) or

TABLE 1. Summary of all radiative forcings calculated for this paper. Uncertainties are given as the interannual confidence intervals with a significance threshold of 95%. The CO_2 concentrations of CO2-4, CO2-8, and CO2-12 are chosen so that the RF_{adj} equal those of ATR-4, ATR-8, and ATR-12 respectively. The uncertainties are smallest for RF_{inst} values and increase for the more complex radiative forcings RF_{adj} and, particularly, ERF.

Name	CO_2 (ppmv)	Air traffic scaling	RF_{inst} (conf) ($W\,m^{-2}$)	RF_{adj} (conf) ($W\,m^{-2}$)	ERF (conf) ($W\,m^{-2}$)
ATR-1	348	1×	—	0.169 (±0.003)	0.019 (±0.129)
ATR-2	348	2×	—	0.274 (±0.003)	—
ATR-4	348	4×	—	0.412 (±0.005)	0.042 (±0.158)
ATR-6	348	6×	—	0.504 (±0.004)	—
ATR-8	348	8×	—	0.595 (±0.008)	0.169 (±0.129)
ATR-10	348	10×	—	0.656 (±0.006)	—
ATR-12	348	12×	0.674 (±0.005)	0.701 (±0.010)	0.261 (±0.102)
CO2-4	373.5 (+25.5)	0×	—	0.403 (±0.000)	0.325 (±0.122)
CO2-8	385 (+37)	0×	—	0.576 (±0.001)	0.439 (±0.152)
CO2-12	393 (+45)	0×	0.413 (±0.000)	0.693 (±0.000)	0.617 (±0.108)
CO2–2×	696 (+348)	0×	2.411 (±0.002)	4.083 (±0.029)	3.548 (±0.124)

CO_2 quadrupling (Vial et al. 2013; Chung and Soden 2015). Due to the fact that the forcing of contrail cirrus is much smaller than $1\,Wm^{-2}$ (see last section) we adopt the concept of running several simulations with gradual upscaling of the largest available aviation inventory (AEDT 2050), by factors of 2 through to 12.

All radiative forcings refer to TOA values. Uncertainties are given as the confidence intervals of annual means on a 95% significance level.

c. *Analysis of rapid radiative adjustments*

Feedback analysis has proven to be a powerful tool in global climate dynamics for unraveling processes that cause climate sensitivity and efficacy differences between different forcings. Most frequently applied to explain the climate sensitivity variation among climate models with respect to a reference CO_2 perturbation (e.g., Bony et al. 2006), the method can as well be used to identify feedback differences occurring between different forcing mechanisms (e.g., Yoshimori and Broccoli 2008; Rieger et al. 2017). Most important for the present study, the method is not only suitable to quantify feedbacks developing in response to surface temperature changes (then usually given in $W\,m^{-2}\,K^{-1}$) but also for calculating rapid radiative adjustments (Vial et al. 2013; Geoffroy et al. 2014; Smith et al. 2018) that contribute to the ERF of some perturbation. Analysis of radiative feedbacks and adjustments can be conducted with two techniques, the partial radiative perturbation (PRP) analysis (e.g., Colman and McAvaney 1997) and the radiative kernel method (e.g., Soden et al. 2008). Use of precalculated kernels derived for a given radiation module implies a basic linearity of radiative fluxes in small parameter changes (Jonko et al. 2012), but it is much more efficient with respect to computational resources. With cloud effects in the focus of this study, and given that obtaining a radiative kernel for clouds is less straightforward than for the other feedback processes (Soden et al. 2008; Klocke et al. 2013), we prefer the PRP method here. An offline radiative transfer scheme for ECHAM5 is available and has been basically described in Klocke et al. (2013) and Rieger et al. (2017). It has been extended for this study to include the effect of contrails as an individual ice cloud component in the calculation of cloud radiative impact (see Bock and Burkhardt 2016b, and references therein).

Rapid adjustments entering contrail cirrus ERF as well as CO_2 ERF will be presented using the output of pairs of simulations, as described in the previous subsection. As recommended in Rieger et al. (2017) two forward and backward PRP calculations are combined to yield one representative value for each rapid adjustment process. Global adjustments to natural cloud changes, lapse rate changes, water vapor changes, and stratospheric temperature changes are accounted for. Results for surface albedo rapid adjustment and Planck adjustment (from surface temperature change extended over the depth of the troposphere) are also calculated, but yield nonzero values only over land, as sea surface temperature and sea ice cannot change in the climate change simulations by construction. Statistical analysis of each radiative adjustment term is done consistently with the treatment of the ERF results derived from the simulations.

3. Results

a. *Radiative forcing estimates*

As described in section 2b air traffic is scaled with gradually increasing factors in order to approach a contrail cirrus amount that results in ERF values that are sufficiently constrained in a statistical sense. Table 1 shows all radiative forcing results that were calculated

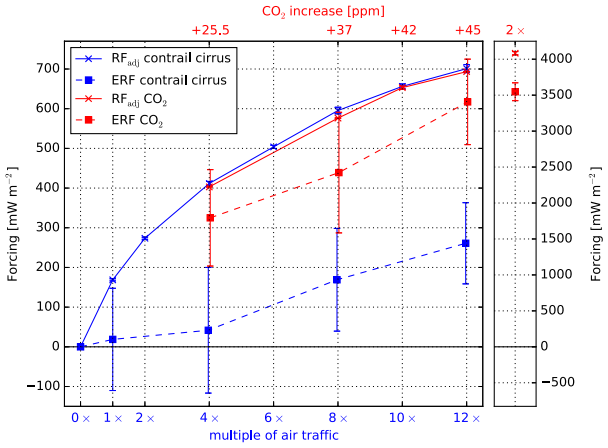

FIG. 1. Radiative forcings from the simulations with different scaling, as done within this project. RF_{adj} (blue solid line) and ERF (blue dashed line) were calculated for different multiples of air traffic based on the AEDT 2050 air traffic dataset. These simulations were accompanied by corresponding CO_2 increase simulations. The CO_2 concentrations were chosen so that the RF_{adj} of CO_2 (red solid line) matches the RF_{adj} of the respective scaled air traffic simulation. ERF simulations for these CO_2 concentrations were performed as well (red dashed line). For evaluating reasons RF_{adj} and ERF were calculated for a CO_2 doubling scenario as well (right box). Error bars are depicted as the 95% confidence interval. Note that the error bars of the RF_{adj} are very small and thus hardly visible.

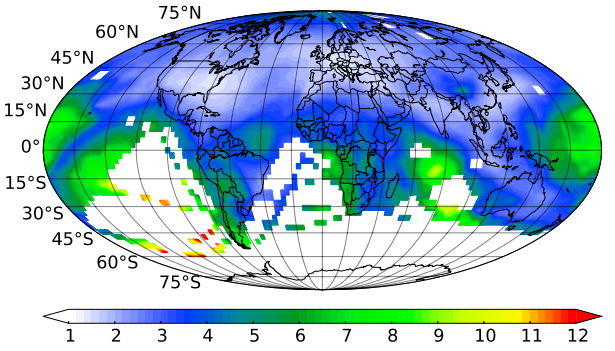

FIG. 2. Maximum-random-overlapped contrail cirrus cover (maximum overlap for connected layers and random overlap for non-connected layers) of ATR-12, divided by that of ATR-1. The result demonstrates the impact of air traffic scaling on contrail cirrus cover. The ratio increases, as a more linear scaling behavior is approached in regions with smaller air traffic in ATR-1 (2050 air traffic).

within this work. The contrail cirrus simulations, yielded with differently scaled AEDT 2050 air traffic, are marked as ATR followed by the scaling factor. In total, seven RF_{adj} simulations and four ERF simulations were performed for contrail cirrus with different scalings between 1 and 12 times air traffic. A corresponding series of simulations was run for CO_2 in order to show a potentially different behavior to contrail cirrus, and to evaluate our model's performance against literature. We performed four RF_{adj} and three ERF simulations for different CO_2 concentrations. The CO_2 concentrations were chosen so that the respective RF_{adj} of CO_2 fits the respective RF_{adj} of contrail cirrus. The ERF simulations of CO_2 use the same concentration changes. These corresponding pairs of CO_2 and contrail cirrus simulations allow us to optimally compare the respective ERFs of air traffic and CO_2 regarding their climate response. The radiative forcings and the respective concentrations of the CO_2 experiments are listed in Table 1. They are marked as CO2 followed by the size of scaling of air traffic which they are supposed to imitate. A CO_2 doubling simulation (CO2-2×) has also been performed for comparison with results available from current literature. RF_{inst} simulations were only performed for ATR-12 and CO2-2×. These values are used for interpreting the results from the adjustment analysis (see section 3b).

Figure 1 shows the radiative forcings of the scaling experiments and includes all RF_{adj} and ERF multiyear mean values and 95% confidence intervals.[1] The RF_{adj} of contrail cirrus for scaled air traffic is depicted in solid blue. All confidence intervals are very small as a result of the radiation double calling technique. The growth of radiative forcing with increasing air traffic is not linear. RF_{adj} for ATR-12 is only about 4 times larger than for ATR-1. This is the result of a gradually increasing saturation effect with respect to contrail cirrus coverage, which is most pronounced in regions where 2050 aviation density is already high. In Fig. 2, which shows the ratio of contrail coverage simulated in ATR-12 and ATR-1, it is obvious that over North America and Europe a 12-fold scaling of aviation density leads to only about twice as much contrail cirrus coverage. In regions less affected by air traffic, like the North Pacific, South America, or Africa, the nonlinearity is less distinct and linear behavior is approached in regions hardly affected by aviation. The saturation-induced nonlinearity is somewhat smaller for RF_{adj} than it is for contrail cirrus coverage (Fig. 3). That is because a further increase of contrail cirrus optical depth (and, thus, of radiative forcing), due to contrail ice crystal nucleation connected with air traffic through aging contrail cirrus, remains possible even if contrail cirrus coverage has reached a maximum value. For a 12× scaling of air traffic (ATR-12) global mean contrail cirrus cover is increased by a factor of 2.7 while global mean RF_{adj} is growing by a factor of 4.1. It is important to note that the zonal structure of contrail cirrus and especially of RF_{adj} is also modified by the scaling. In ATR-10 and ATR-12, a second (tropical)

[1] Note that all confidence intervals indicating uncertainty of mean values refer to statistical uncertainty. No measures are given for physical uncertainty with respect to models, parameterizations, etc.

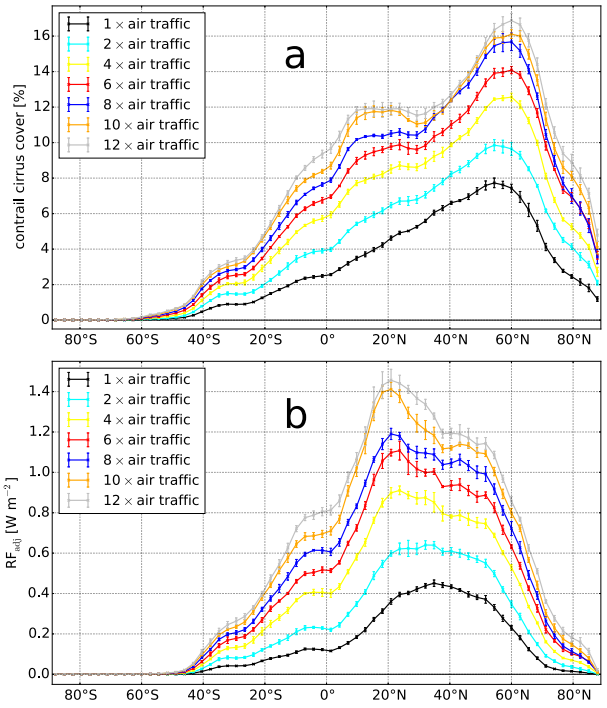

FIG. 3. Zonal profile of (a) maximum-random-overlapped contrail cirrus cover and (b) RF_{adj} for different scalings of air traffic. The results are based on the RF_{adj} simulations displayed in Fig. 1. Error bars show the 95% confidence interval.

contrail cirrus maximum shows up that is not apparent in ATR-1 (Fig. 3a). While the relative maxima of zonal mean contrail cirrus coverage and zonal mean RF_{adj} largely coincide in any scaling experiment, it is obvious that a gradual shift of the absolute maximum RF_{adj} occurs with the scaling, with highest radiative forcing for fourfold (and higher) scaling showing up around 20°N (Fig. 3b). For ATR-1 and ATR-2, in contrast, there is rather a broad RF_{adj} maximum between 20° and 55°N. This feature strongly suggests a higher net radiative impact per unit cirrus coverage in subtropical latitudes than in midlatitudes. We will return to this finding when discussing, in section 4, the possibility to transfer conclusions from the heavily scaled simulations to the nonscaled case of 2050 air traffic.

The respective ERFs of air traffic (blue dashed line, Fig. 1) are substantially lower than RF_{adj} (e.g., about 11% and 37% for mean RF_{adj} in ATR-1 and ATR-12, respectively). Note that the confidence intervals are now more than one magnitude larger than for RF_{adj}. This implies that although all contrail cirrus multiyear mean ERFs are positive, only the values for ATR-8 and ATR-12 can be regarded as significantly larger than zero. However, for all simulations the ERF is found to be significantly lower than RF_{adj}. Disregarding ATR-1 and ATR-4, where the mean value is smaller than the confidence interval, we conclude from the more significant results from ATR-8 and ATR-12 that contrail cirrus ERF is reduced to between 25% and 35% of its corresponding RF_{adj}.

Since some previous studies, notably Forster et al. (2016), have indicated ERF to be smaller than RF_{adj} for CO_2 as well, our second simulation series compares the amount of relative ERF reduction in contrail cirrus and CO_2 increase simulations. Hence, as described in section 2b, the CO_2 concentrations of the RF_{adj} for increased CO_2 were chosen to equal RF_{adj} of one corresponding contrail cirrus case. The resulting RF_{adj} for CO_2 is depicted in Fig. 1 by the red solid line. CO_2 concentrations between +25.5 ppmv (corresponding to ATR-4) and +45.0 ppmv (corresponding to ATR-12) were utilized and cause RF_{adj} in the CO_2 simulation series to match their respective ATR counterparts within a 3% range. The confidence intervals are similarly narrow for the RF_{adj} in CO2-n and ATR-n. For the same reason as for the ATR series, the confidence intervals are much larger for the ERFs. The ERFs are consistently lower than the respective RF_{adj} of CO_2 but the difference just fails to yield significance on the 95% level. A significant decrease, however, is reached for CO2-2× (right box of Fig. 1). Here, the ERF is lower by about 13% than RF_{adj}, largely consistent with the respective difference of near 10% for CO2-12.

In all simulations the drop of ERF relative to RF_{adj} is stronger for the ATR than for the CO_2 simulations. Especially for ATR-12, this difference is significant. It is, hence, promising to make an attempt for explaining the origin of the difference by feedback analysis (Rieger et al. 2017).

b. *Adjustment analysis*

The previous subsection has revealed a substantial ERF reduction, compared to the RF_{adj}, for the ATR simulations. In this subsection we address the physical background of this reduction and the difference to the CO_2 case. The method of PRP feedback analysis is applied to ATR-12 and CO2-2× in order to determine the rapid adjustments. The sum of all rapid adjustments is expected to explain the difference between ERF and RF_{inst}. However, as for various reasons (Boer and Yu 2003; Rieger et al. 2017) they can never match exactly, the deviation is depicted as a residuum. We utilize the two runs with the largest scalings because they most likely will yield statistically significant results. Hence, CO2-2× is preferred over CO2-12, an option that can be justified by the quantitatively similar relative ERF reduction in these two cases (see Table 1).

Figure 4 shows the results of the adjustment analysis of ATR-12. Note that the RF_{adj} is shown here instead of

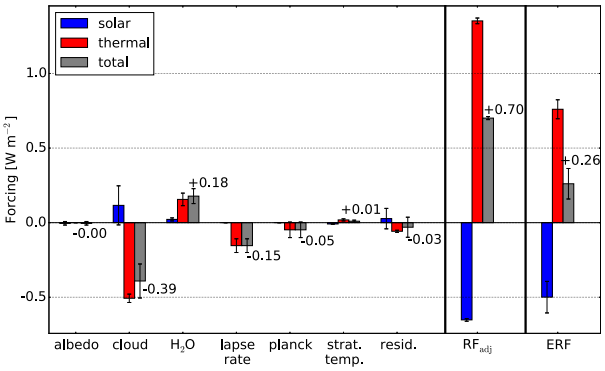

FIG. 4. Results of the adjustment analysis of ATR-12 (left box), with the respective rapid radiative adjustments including residuum, the RF_{inst} (middle box), and the ERF (right box). The total forcings (gray bars) are split into a shortwave part (blue bars) and a longwave part (red bars). Error bars show the 95% confidence interval.

RF_{inst}, which would formally be most consistent because all rapid adjustments from the PRP analysis are instantaneous changes at the TOA. However, the sum of RF_{inst} and the stratospheric temperature adjustment yields RF_{adj} (Table 1). As already known from Dietmüller et al. (2016), the stratospheric temperature adjustment from contrail cirrus is small. In the case discussed here (i.e., ATR-12) it is less than 4% of RF_{inst}. If the rapid adjustments including residuum (left box) are added to the RF_{adj} (mid box) the ERF is yielded (right box).

As explained in section 2b, there is a small surface temperature response in the fixed SST simulations and, thus, a nonzero Planck feedback. However, this one as well as the surface albedo feedback are small and contribute little to the total rapid radiative adjustment. For ATR-12, a global mean surface temperature response of only +0.012 K has been calculated, nearly matching the fixed SST criteria. The other adjustment components are much more substantial (and also statistically significant). The lapse rate and water vapor adjustment, which both are directly or indirectly induced by tropospheric temperature changes, nearly compensate each other. Hence, the cloud adjustment, which almost equals the total decrease of ERF of about $-413\,\mathrm{mW\,m^{-2}}$, is mainly responsible for the large ERF reduction. With $-31\,\mathrm{mW\,m^{-2}}$, the residuum turns out to be quite small, which confirms a consistent analysis.

The rapid radiative adjustments can be explained by the change of patterns of the basic parameters. Figure 5d shows the temperature change of ATR-12. The typical dipole effect induced by contrail cirrus can be noticed, with cooling above and warming below those regions where contrail cirrus occurs (Ackerman et al. 1988; Ponater et al. 2005). The cooling above the contrail

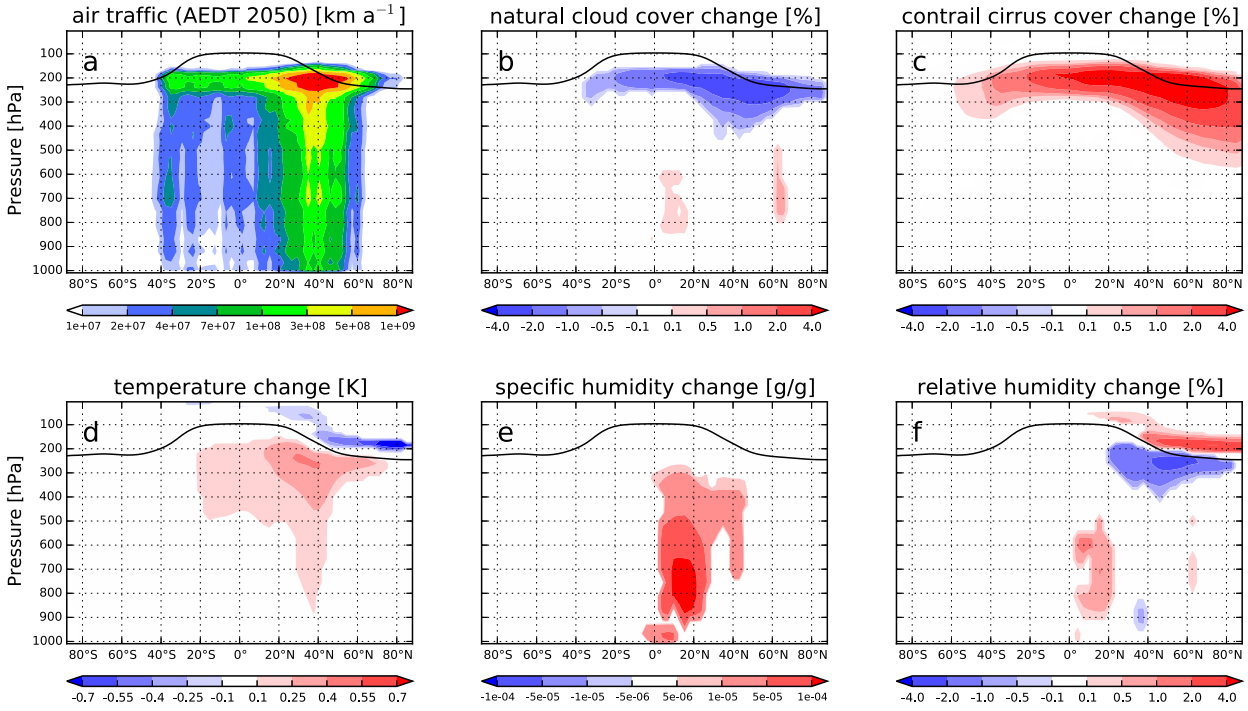

FIG. 5. Zonal mean vertical cross section of (a) air traffic, (b) absolute natural cloud cover change, (c) absolute contrail cirrus cover change, (d) temperature change, (e) specific humidity change, and (f) absolute change of relative humidity for ATR-12. Data are only plotted for areas where the deviation from the reference is significant to the 95% confidence interval.

cirrus in the northern extratropics causes less upward longwave radiation and, thus, a slightly positive stratospheric temperature adjustment. In the troposphere a warming can be observed with a maximum just below the main flight levels (cf. Figs. 5a and 5d). The warming decreases with decreasing height and becomes almost zero on the surface. This temperature increase with height leads to a negative lapse rate adjustment because the higher and warmer levels emit more longwave radiation. It is common in feedback analysis to find the (negative) lapse rate feedback associated with an overcompensating positive water vapor feedback. There is indeed a tropospheric water vapor increase between 0° and 45°N in ATR-12 (Fig. 5e), yet only below 300 hPa it is significant. At aviation cruise altitudes, between 20° and 80°N, the relative humidity even decreases slightly, by about 4% (Fig. 5f). Enhanced contrail cirrus formation evidently leads to local dehydration of ambient air, as pointed out in Burkhardt and Kärcher (2011) and Schumann et al. (2015). While little contribution of the respective regions to the water vapor adjustment can thus be expected, still the combined effect of lapse-rate and water vapor adjustment remains slightly positive.

The cloud adjustment ($-391\,\mathrm{mW\,m^{-2}}$) contributes by far the largest adjustment component in ATR-12. A closer look at the contributions to cloud cover change (see Figs. 5b and 5c) reveals that the contrail cirrus cover increase is accompanied and partly compensated by a decrease in the cover of natural cirrus clouds. This effect is most distinct in regions with high air traffic density (cf. to Fig. 5a). For example at the 220-hPa level a contrail cirrus cover of +3.5% faces a loss of natural cirrus cover of −1.4% (percentage points). This compensation effect becomes stronger for larger scalings because the relative decrease of natural cloud cover is larger in that case. In contrast to the rapid radiative cloud adjustment, the change of contrail and cirrus coverage at flight level (Figs. 5b,c) is statistically significant, even with lower scaling factors. At 220 hPa about 41% of the contrail cirrus cover is compensated by a loss of natural cirrus cover for ATR-12, while for ATR-1 only 34% are compensated. Still, these values just may mark an upper limit, because they refer to the 220-hPa level where the highest air traffic density occurs. Overall, the contrail cover reduction numbers suggest a smaller ERF reduction for less scaled air traffic, but this is largely obscured for ATR-1 due to excessive statistical noise.

The significant radiative adjustments showing up in ATR-12 have hardly any respective counterpart in CO2-12 (not shown), thus explaining why in the latter case the difference between RF_{adj} and ERF (about 10%) is only marginally significant. Specific conclusions with respect to individual adjustment components are not possible for CO2-12 due to the high statistical uncertainty. However, we use the results yielded for CO2-2× to point out that a significant reduction of ERF also shows up in the CO_2 case, although much smaller than for contrail cirrus. At the same time a closer look at our CO_2 adjustments allows a comparison with respective literature results, which is not possible for contrail cirrus as it is analyzed for the first time in the present paper.

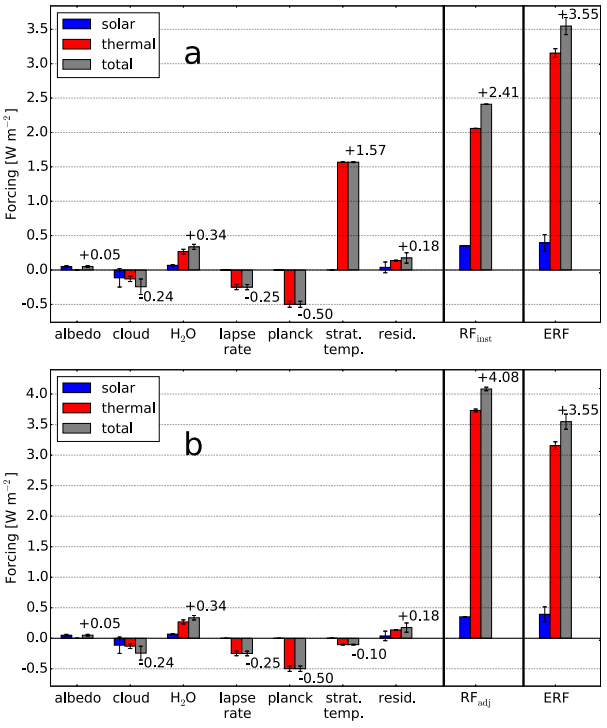

FIG. 6. The plots show the adjustment analysis of CO2-2× with the respective rapid radiative adjustments including residuum (left boxes) and ERF (right boxes); (a) is created in the same way as Fig. 4, whereas in (b) the RF_{inst} is replaced by the RF_{adj} (middle boxes) in order to emphasize the remaining stratospheric temperature adjustment ($-0.1\,\mathrm{mW\,m^{-2}}$) after removal of the component directly induced by the CO_2 increase. This remaining stratospheric temperature adjustment is accounted for by the PRP analysis, but not by the RF_{adj} calculations that uses the radiation double calling technique. The respective forcings (gray bars) are subdivided into a shortwave part (blue bars) and a longwave part (red bars). Error bars show the 95% confidence interval.

The CO_2 adjustment analysis results for CO2-2× are shown in Fig. 6. Unlike the contrail cirrus case, global mean surface temperature markedly increases (+0.164 K), leading to a significant negative Planck adjustment. This is accompanied by a decrease of the global snow coverage, leading to a slightly positive surface albedo adjustment. These features are fully consistent with results reported in Smith et al. (2018, their Figs. S3 and S7), which have been calculated applying the kernel method

on a variety of climate models. As usual for a CO_2 increase, stratospheric temperatures, in particular above 70 hPa, decrease in CO2-2× (not shown here), resulting in a large positive stratospheric temperature adjustment. This stratospheric temperature adjustment is largely included in the RF_{adj} (Fig. 6). Only a small part of the stratospheric temperature adjustment resulting from the PRP analysis is not induced directly by the CO_2 increase (Fig. 6b). As already discussed above, tropospheric temperatures qualitatively control the water vapor and lapse rate adjustments. Tropospheric temperatures increase throughout the whole troposphere by about 0.05 to 0.1 K with the largest warming found at 750 hPa, inducing a significantly negative lapse rate adjustment. Correlated with the tropospheric warming a water vapor increase can be noticed, as usual (not shown here). The resulting enhanced greenhouse effect is reflected by a positive water vapor adjustment. More distinct than for the contrail cirrus case (ATR-12), the water vapor adjustment exceeds the lapse rate adjustment in magnitude.

The cloud adjustment is negative and has the largest statistical uncertainty of all individual adjustment components. Both parts, the solar as well as the thermal, are negative. The negative solar contribution is largely driven by a minimum of cloud adjustment in the tropical region of the Atlantic between 5°S and 20°N. The main reason for this minimum is an increase of low-level cloud cover over the tropical Atlantic (not shown here). The stratospheric temperature adjustment is the largest individual component, but if only tropospheric effects are considered the total adjustment is negative, consistent with Fig. 1. Except for the negative cloud adjustment, all these findings are largely in agreement with Smith et al. (2018, their Fig. 3).

4. Discussion

The central finding reported here is a substantial reduction of contrail cirrus ERF, in comparison to RF_{adj}, mainly caused by a negative radiative adjustment from natural clouds. This is physically consistent because the parameterized contrail cirrus is fully embedded in the hydrological cycle (Bock and Burkhardt 2016a), so a considerable amount of water vapor in the upper troposphere is removed by condensation inside the forming and developing contrail cirrus. Respective evidence is obvious in the simulated relative humidity and natural cloud cover (Figs. 5f and 5b), as also pointed out previously by Burkhardt and Kärcher (2011, their Fig. 4a). Water vapor decrease and a redistribution of water condensate from the upper atmosphere to lower altitudes by the presence of contrail cirrus have also been identified in an independent climate model setup described by Schumann et al. (2015). Qualitatively, the mechanism has also been noticed in less parameterized models like the high-resolution contrail model of Unterstrasser et al. (2017), where particularly for slow updraft velocities contrail cirrus fully develops before natural cloud formation starts, thus removing supersaturated water vapor from the atmosphere. However, natural cirrus formation is also hampered by simple geometrical displacement in these simulations. Likewise, in simulations with the high resolution regional-scale climate model COSMO-ART (Gruber et al. 2018) evidence has been found to support a reduction of the ice water path of natural cirrus, if contrail formation preceded natural cloud formation (Gruber 2015, his Fig. 4.7).

While the qualitative phenomenon of reduced natural cirrus formation in an atmosphere affected by aviation is both plausible and supported by previous research, harder to answer is the question whether the natural cirrus adjustment is able to compensate as much as two-thirds of the radiative forcing of contrails. This is a much larger reduction effect than estimated in Burkhardt and Kärcher (2011) although a similar contrail cirrus parameterization has been used. The difference may partly be attributable simply to the scaling (see below). However, part of the deviation can be explained by a different methodology. In the present paper the cloud adjustment is determined directly from the radiative effect of cloud changes all over the troposphere, including contributions from altitudes below flight level (Fig. 5b). This approach differs from that used in Burkhardt and Kärcher (2011), who had only one simulation with unscaled aviation available and projected a 20% radiative forcing reduction from natural cloud cover changes directly downstream of the main contrail cirrus regions.

It is tempting to quote the results from Chen and Gettelman (2013, 2016) in quantitative support of the evidence yielded here. Those studies used an radiative forcing calculation approach similar to ours, finding radiative forcing values at least 50% smaller than all other available estimates of instantaneous or stratosphere adjusted RF from contrail cirrus. Chen and Gettelman used specified dynamics simulations (''nudging''), which lead to a better signal-to-noise ratio than free-running simulations (Forster et al. 2016), and allowed them to refrain from the strong aviation scaling that we inevitably have to use for the present study. However, as also pointed out by Forster et al. (2016), the nudging procedure might well obscure part of the atmospheric adjustments and is, hence, unlikely to form a fully valid method for ERF calculation. At the same time, there are profound differences in the microphysical treatment of contrail formation in ECHAM5-CCMod and CAM5

(Bock and Burkhardt 2016a; Chen and Gettelman 2013, respectively), indicating that the lower radiative effect of the CAM5 contrails may as well have its origin in lower initial ice crystal numbers simulated in that model [see discussion in Bock and Burkhardt (2019)]. Hence, a straightforward attribution of the discrepancy between the radiative impact estimates to the RF calculation method is not possible. Unfortunately, the existing observation-based studies addressing the radiative effect of contrails cirrus (Graf et al. 2012; Minnis et al. 2013; Vázquez-Navarro et al. 2015) also do not help to constrain the ERF, as they apply detection criteria to separate aviation-induced cirrus from natural cirrus, which most likely do not cover the natural cirrus adjustments simulated by the climate models.

Ponater (2010) found a reduced efficacy of line-shaped contrails even in simulations neglecting the feedback of contrails to their environment through removing water vapor from the ambient atmosphere. The temperature response pattern found in the present study (Fig. 5d) in fact indicates a stabilizing effect near the tropopause. First, this may have a slight damping effect on natural cloud formation, even in the absence of reduced supersaturation available for condensation. Second, it will in any case induce a negative lapse rate adjustment. Indeed, the lapse rate adjustment is relatively large for ATR-12 (20% magnitude of the RF_{adj}, compared to respective 6% for CO2-2×). However, lapse rate feedback and water vapor feedback are known to be intimately coupled, partly compensating each other (e.g., Cess 1975; Bony et al. 2006). This feature apparently holds for rapid radiative adjustments as well (Smith et al. 2018, their Fig. S7). We find the combined water vapor–lapse rate adjustment less positive for contrail cirrus than for the CO_2, so this effect makes a moderate contribution to the stronger ERF reduction in the former case. From simulations with a column model accounting for radiation and vertical mixing, Schumann and Mayer (2017) have deduced a potentially weak impact of upper tropospheric cirrus on surface temperature, which they relate to a faster radiative energy loss to space (compared to the mixing time scale) for this particular forcing mechanism. The temperature response profile forced by cirrus in their simulations partly resembles the respective pattern forced by contrails in our Fig. 5d (see also Ponater et al. 2005, their Fig. 2). From an equilibrium perspective, a temperature profile change of this kind induces an enhanced negative lapse rate feedback, potentially explaining a weakened or missing surface warming. However, the column model of Schumann and Mayer (2017) does not include water vapor or background cloud adjustments. Thus it represents only one aspect of the contrail impact on troposphere/surface heating and cannot quantify the balance of effects actually responsible for an ERF reduction.

If the evidence of such a strong natural cloud adjustment as found in our scaled contrail cirrus simulations is realistic, can it be safely assumed to hold for the unscaled case as well? As is obvious from the results (Fig. 3), a shift of the contrail cirrus cover and ERF toward lower latitudes occurs as a consequence of the scaling. The same shift may occur for the natural cloud adjustment, with the net radiative impact per unit cirrus cover being larger in tropical than in midlatitudes. Hence, the compensation effect between contrail cirrus radiative forcing and natural cirrus adjustment might be enhanced for heavily scaled aviation. From our simulation series, there is little evidence to support this, yet the cloud radiative adjustment for the simulations involving little scaling is too noisy to draw definite conclusions. Nevertheless, and because the underlying physical processes remain comparable, we expect a substantial ERF reduction also for unscaled air traffic inventories.

Most recently, amendments have been implemented in the contrail cirrus parameterization that account for the dependence of ice nucleation on ambient temperature (Kärcher et al. 2015). Respective simulations indicate that the parameterization used here leads to considerable overestimation of ice crystal numbers at tropical latitudes. This implies, according to Burkhardt et al. (2018), that in this study we overestimate lifetime and radiative forcing of tropical contrail cirrus, also potentially overrating its power to feedback on adjacent natural cirrus.

In the framework of the present study the CO_2 simulations only serve as a reference case that allows us to identify the peculiarities of contrail cirrus induced radiative adjustments. We are, therefore, not particularly worried about the only marginally (or missing) statistical significance of rapid adjustments contributing to the apparent ERF reduction in, for example, the CO2-12 simulation. The qualitative findings are consistent throughout the series of CO_2 simulations (including CO2-2×), and the ERF reduction is clearly and significantly stronger in the contrail cirrus case. Nevertheless, the fact that the PRP feedback analysis yields a negative cloud radiative adjustment for CO2-2× deserves some extra consideration, as previous results (e.g., Vial et al. 2013; Smith et al. 2018) suggest a positive contribution in comparable multimodel CO_2 increase studies. Being somewhat beyond the main topic of our paper, this aspect is extended in some detail only in the appendix below.

5. Conclusions and outlook

Based on a well-approved climate model using a state-of-the-art contrail cirrus parameterization, this study

finds the effective radiative forcing (ERF) of contrail cirrus to be more than 50% smaller than the corresponding stratosphere adjusted radiative forcing. To yield statistically significant ERF results air traffic volume had to be scaled severely, and even with a scaling factor 12 the 95% confidence interval ranges from 49% to 77% reduction with a mean value of roughly 65%. Despite such considerable uncertainty it is obvious that the reduction of contrail cirrus ERF is much larger than it is in case of a CO_2 forcing of similar magnitude, a finding that holds for the less scaled simulations, too. Hence, we deem it tenable to assume an ERF reduction by about 35% of the associated conventional RF for the unscaled 2050 and even 2006 aviation cases as well. By all means that makes a more reasonable estimate than assuming the same value for ERF and RF_{adj}. An analysis of all radiative adjustments contributing to contrail cirrus ERF indicates that the main reason of the reduction is a counteracting response of the natural cloud radiative effect, which decreases as contrail cirrus develops. In comparison to CO_2 forcing, an increased (negative) lapse rate adjustment is also found, but this contribution is less important than the cloud adjustment.

The conclusions of this paper are strongly suggestive of a low efficacy of contrail cirrus to force a global mean surface temperature increase, thereby confirming earlier findings for line-shaped contrails (Ponater et al. 2005; Rap et al. 2010). However, such an inference should not be made prematurely. Although ERF is generally considered to be a good metric to quantitatively intercompare various forcing agents and to predict the expected surface temperature response, a certain level of efficacy fluctuation has also been reported within the ERF framework (e.g., Shine et al. 2012; Marvel et al. 2016). Forcings mainly originating from the northern extratropics, such as contrail cirrus, are rather prone to higher efficacy (e.g., Berntsen et al. 2005; Shindell 2014). The next step to this study will be, hence, direct simulation of the surface temperature change from contrail cirrus with a coupled atmosphere–ocean model. We will use a corresponding approach with scaled air traffic as an input, profiting from the experience that is documented here.

Another note of caution is also sensible, because the results in the present study are derived from one climate model only. In CO_2-driven simulations, cloud adjustments and feedbacks have been known to differ strongly between models, with high clouds contributing particularly strong to the intermodel spread (Zelinka et al. 2013). Several ongoing research programs attempt to advance the respective process understanding (e.g., Webb et al. 2017). Even less is known on cloud adjustments and feedbacks in simulations driven by non-CO_2 forcings, and (in the absence of other respective studies) we cannot say anything about the robustness of model simulated cloud adjustments to contrail cirrus occurrence. Development of more and independent climate model setups to support the evidence presented here is thus highly desirable.

Acknowledgments. This work received dedicated funding from the DLR aeronautics board (Ph.D. project "Efficacy of Contrail Cirrus"). We are very grateful to Vanessa Rieger (DLR) for the assistance regarding the PRP method. We thank Johannes Quaas (University of Leipzig) and Robert Sausen (DLR) for the fruitful discussions and support. Further, we thank Simon Unterstrasser (DLR) as well as Christopher Smith (University of Leeds) and another anonymous reviewer for thoughtful comments and remarks, which helped to improve this publication. We gratefully acknowledge the computational resources provided by the German Climate Computing Center (DKRZ).

APPENDIX

Potential Origins of a Negative Cloud Radiative Adjustment to CO_2 Increase

As pointed out in section 3b the results of the adjustment analysis for CO_2 doubling (see Fig. 6) are generally in good agreement with literature. However, our cloud adjustment of CO2-2× is negative ($-0.244\,W\,m^{-2}$), which seems inconsistent with positive values almost throughout the literature (e.g., Vial et al. 2013; Zelinka et al. 2013; Smith et al. 2018). A closer look reveals that our shortwave cloud adjustment ($-0.114\,W\,m^{-2}$) is the main reason for this finding, while the longwave part ($-0.130\,W\,m^{-2}$) is well within the expected range [compared to Vial et al. (2013, their Table 2) and Smith et al. (2018, their Fig. 4)]. Further analysis of spatial distributions (not shown here) indicates that the excessive negative shortwave cloud adjustment originates from a clearly defined region in the tropical Atlantic that is characterized by an increase of low cloud cover. In that region our results differ from comparable distributions shown by, for example, Zelinka et al. (2013, their Fig. 9b), while there is an overall pattern consistency over the rest of the globe. We also remark that large intermodel differences for cloud rapid adjustments, even in sign, have been pointed out before in literature [see Vial et al. (2013, their Table 2)].

However, variations of rapid radiative adjustments results do not only originate from intermodel differences, but may also show up from the application of different calculation methods. We apply the PRP method in its centered version, where the forward and backward calculations are combined, as strongly recommended by

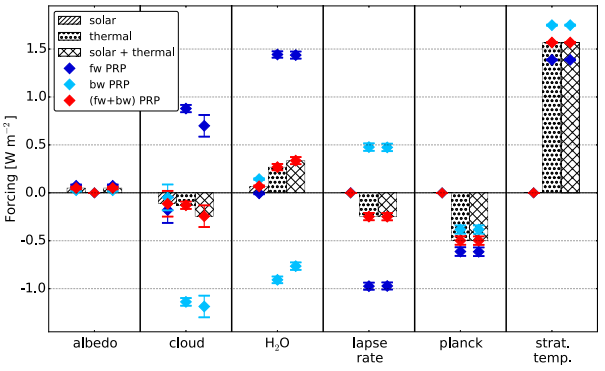

FIG. A1. Results for the radiative adjustment analysis of CO2-2×, as in Fig. 6a, but with the respective PRP forward (dark blue), backward (light blue), and centered (red) results. The total forcings (crossed infill) are subdivided into a shortwave part (striped infill) and a longwave part (dotted infill). Error bars show the 95% confidence interval.

Klocke et al. (2013) and Rieger et al. (2017) for feedback analysis of ocean-coupled simulations. Our Fig. 6, as well as results shown in Rieger et al. (2017, their Fig. 4), indicate general consistency with previous work, except for the shortwave cloud adjustment discussed above. However, in the rather low number of publications where the PRP method is utilized, almost exclusively slow feedbacks have been calculated. Most studies prefer the more resource efficient kernel method where the cloud adjustment is usually approximated via the cloud radiative effect (CRE), corrected for the cloudy-sky parts of the remaining adjustments [also known as the ''kernel difference method'' after Smith et al. (2018)]. This implies that a potential cloudy-sky residuum is included in the cloud adjustment. Obtaining cloud kernels is possible as well (Zelinka et al. 2012) but the technique is not as straightforward as for the other feedback processes. Overall, the residual terms of the kernel method [see Vial et al. 2013, their Table 2)] tend to be larger than those shown here. The linearity assumption for kernels is fulfilled for small perturbations, as used here, but kernels should be chosen carefully when approaching larger scalings (Jonko et al. 2012). What is obvious, however, when looking at the PRP results for rapid radiative adjustments, is the large difference between forward and backward calculation for the cloud, water vapor, and lapse rate case (see Fig. A1). Kernels are usually set up in a way that corresponds to the forward calculation of the PRP method, by using an incremental parameter perturbations added to the reference state. This could well lead to systematic disagreements when comparing PRP and kernel results, as confirmed by a closer study of the results given by Klocke et al. (2013, their Table 1). We therefore suggest that testing of a corresponding forward/backward analysis approach could be worthwhile for the kernel method as well.

Finally, in order to explain the large variability of cloud adjustments it might also be very useful to include the International Satellite Cloud Climatology Project (ISCCP) simulator diagnostics in further studies [as recommended by Smith et al. (2018)].

REFERENCES

Ackerman, T. P., K.-N. Liou, F. P. J. Valero, and L. Pfister, 1988: Heating rates in tropical anvils. *J. Atmos. Sci.*, **45**, 1606–1623, https://doi.org/10.1175/1520-0469(1988)045<1606:HRITA>2.0.CO;2.

Berntsen, T. K., and Coauthors, 2005: Response of climate to regional emissions of ozone precursors: Sensitivities and warming potentials. *Tellus*, **57B**, 283–304, https://doi.org/10.3402/tellusb.v57i4.16549.

Bier, A., and U. Burkhardt, 2019: Variability in contrail ice nucleation and its dependence on soot number emissions. *J. Geophys. Res.*, **124**, 3384–3400, https://doi.org/10.1029/2018JD029155.

Bock, L., and U. Burkhardt, 2016a: The temporal evolution of a long-lived contrail cirrus cluster: Simulations with a global climate model. *J. Geophys. Res.*, **121**, 3548–3565, https://doi.org/10.1002/2015JD024475.

——, and ——, 2016b: Reassessing properties and radiative forcing of contrail cirrus using a climate model. *J. Geophys. Res.*, **121**, 9717–9736, https://doi.org/10.1002/2016JD025112.

——, and ——, 2019: Contrail cirrus radiative forcing for future air traffic. *Atmos. Chem. Phys.*, **19**, 8163–8174, https://doi.org/10.5194/ACP-19-8163-2019.

Boer, G. J., and B. Yu, 2003: Climate sensitivity and climate state. *Climate Dyn.*, **21**, 167–176, https://doi.org/10.1007/S00382-003-0323-7.

Bony, S., and Coauthors, 2006: How well do we understand and evaluate climate change feedback processes? *J. Climate*, **19**, 3445–3482, https://doi.org/10.1175/JCLI3819.1.

Boucher, O., and Coauthors, 2013: Clouds and aerosols. *Climate Change 2013: The Physical Science Basis*, T. F. Stocker et al., Eds., Cambridge University Press, 571–657.

Brasseur, G. P., and Coauthors, 2016: Impact of aviation on climate: FAA's Aviation Climate Change Research Initiative (ACCRI) Phase II. *Bull. Amer. Meteor. Soc.*, **97**, 561–583, https://doi.org/10.1175/BAMS-D-13-00089.1.

Burkhardt, U., and B. Kärcher, 2009: Process-based simulation of contrail cirrus in a global climate model. *J. Geophys. Res.*, **114**, D16201, https://doi.org/10.1029/2008JD011491.

——, and ——, 2011: Global radiative forcing from contrail cirrus. *Nat. Climate Change*, **1**, 54–58, https://doi.org/10.1038/nclimate1068.

——, L. Bock, and A. Bier, 2018: Mitigating the contrail cirrus climate impact by reducing aircraft soot number emissions. *npj Climate Atmos. Sci.*, **1**, 37, https://doi.org/10.1038/S41612-018-0046-4.

Cess, R. D., 1975: Global climate change: An investigation of atmospheric feedback mechanisms. *Tellus*, **27**, 193–198, https://doi.org/10.3402/tellusa.v27i3.9901.

Chen, C., and A. Gettelman, 2013: Simulated radiative forcing from contrails and contrail cirrus. *Atmos. Chem. Phys.*, **13**, 12 525–12 536, https://doi.org/10.5194/acp-13-12525-2013.

——, and ——, 2016: Simulated 2050 aviation radiative forcing from contrails and aerosols. *Atmos. Chem. Phys.*, **16**, 7317–7333, https://doi.org/10.5194/acp-16-7317-2016.

Chen, N. Y., B. Sridhar, and H. K. Ng, 2012: Tradeoff between contrail reduction and emissions in United States national

airspace. *J. Aircr.*, **49**, 1367–1375, https://doi.org/10.2514/1.C031680.

Chung, E.-S., and B. J. Soden, 2015: An assessment of direct radiative forcing, radiative adjustments, and radiative feedbacks in coupled ocean–atmosphere models. *J. Climate*, **28**, 4152–4170, https://doi.org/10.1175/JCLI-D-14-00436.1.

Colman, R., and B. J. McAvaney, 1997: A study of GCM climate feedbacks from perturbed SST experiments. *J. Geophys. Res.*, **102**, 19 383–19 402, https://doi.org/10.1029/97JD00206.

Dahlmann, K., V. Grewe, C. Frömming, and U. Burkhardt, 2016: Can we reliably assess climate mitigation options for air traffic scenarios despite large uncertainties in atmospheric processes? *Transport. Res.*, **46D**, 40–55, https://doi.org/10.1016/J.TRD.2016.03.006.

Dietmüller, S., and Coauthors, 2016: A new radiation infrastructure for the modular Earth submodel system (MESSy, based on version 2.51). *Geosci. Model Dev.*, **9**, 2209–2222, https://doi.org/10.5194/gmd-9-2209-2016.

FESG, 1998: Report of the Forecasting and Economic Support Group (FESG): Long-range scenarios. Tech. Rep. 4, International Civil Aviation Organization Committee on Aviation Environmental Protection Steering Group, Montreal, Canada, 131 pp.

Forster, P., R. S. Freckleton, and K. P. Shine, 1997: On aspects of the concept of radiative forcing. *Climate Dyn.*, **13**, 547–560, https://doi.org/10.1007/s003820050182.

——, and Coauthors, 2016: Recommendations for diagnosing effective radiative forcing from climate models for CMIP6. *J. Geophys. Res.*, **121**, 12 460–12 475, https://doi.org/10.1002/2016JD025320.

Geoffroy, O., D. Saint-Martin, A. Voldoire, D. Salas y Melia, and S. Senesi, 2014: Adjusted radiative forcing and global radiative feedbacks in CNRM-CM5, a closure of the partial decomposition. *Climate Dyn.*, **42**, 1807–1818, https://doi.org/10.1007/s00382-013-1741-9.

Gettelman, A., and C. Chen, 2013: The climate impact of aviation aerosols. *Geophys. Res. Lett.*, **40**, 2785–2789, https://doi.org/10.1002/grl.50520.

Giorgetta, M. A., G. P. Brasseur, E. Roeckner, and J. Marotzke, 2006: Preface to special section on climate models at the Max Planck Institute for Meteorology. *J. Climate*, **19**, 3769–3770, https://doi.org/10.1175/JCLI9023.1.

Graf, K., U. Schumann, H. Mannstein, and B. Mayer, 2012: Aviation induced diurnal North Atlantic cirrus cover cycle. *Geophys. Res. Lett.*, **39**, L16804, https://doi.org/10.1029/2012GL052590.

Gregory, J. M., and Coauthors, 2004: A new method for diagnosing radiative forcing and climate sensitivity. *Geophys. Res. Lett.*, **31**, L03205, https://doi.org/10.1029/2003GL018747.

Grewe, V., and Coauthors, 2017: Mitigating the climate impact from aviation: Achievements and results of the DLR WeCare project. *Aerospace*, **40**, 2785–2789, https://doi.org/10.3390/aerospace4030034.

Gruber, S., 2015: Simulating contrails and their impact on incoming solar radiation at the surface on the regional scale—A case study. Master's thesis, Department of Troposphere Research, Karlsruhe Institute of Technology, 97 pp.

——, S. Unterstrasser, J. Bechtold, H. Vogel, M. Jung, H. Pak, and B. Vogel, 2018: Contrails and their impact on shortwave radiation and photovoltaic power production—A regional model study. *Atmos. Chem. Phys.*, **18**, 6393–6411, https://doi.org/10.5194/acp-18-6393-2018.

Hansen, J., M. Sato, and R. Ruedy, 1997: Radiative forcing and climate response. *J. Geophys. Res.*, **102**, 6831– 6864, https://doi.org/10.1029/96JD03436.

——, and Coauthors, 2005: Efficacy of climate forcings. *J. Geophys. Res.*, **110**, D18104, https://doi.org/10.1029/2005JD005776.

IPCC, 2013: *Climate Change 2013: The Physical Science Basis.* T. F. Stocker et al., Eds., Cambridge University Press, 1535 pp.

Jonko, A. K., K. M. Shell, B. M. Sanderson, and G. Danabasoglu, 2012: Climate feedbacks in CCSM3 under changing CO_2 forcing. Part I: Adapting the linear radiative kernel technique to feedback calculations for a broad range of forcings. *J. Climate*, **25**, 5260–5272, https://doi.org/10.1175/JCLI-D-11-00524.1.

Joshi, M., K. P. Shine, M. Ponater, N. Stuber, R. Sausen, and L. Li, 2003: A comparison of climate response to different radiative forcings in three general circulation models: Towards an improved metric of climate change. *Climate Dyn.*, **20**, 843–854, https://doi.org/10.1007/s00382-003-0305-9.

Kärcher, B., 2017: Cirrus clouds and their response to anthropogenic activities. *Curr. Climate Change Rep.*, **3**, 45–57, https://doi.org/10.1007/S40641-017-0060-3.

——, 2018: Formation and radiative forcing of contrail cirrus. *Nat. Commun.*, **9**, 1824, https://doi.org/10.1038/s41467-018-04068-0.

——, U. Burkhardt, S. Unterstrasser, and P. Minnis, 2009: Factors controlling contrail cirrus optical depth. *Atmos. Chem. Phys.*, **9**, 6229–6254, https://doi.org/10.5194/acp-9-6229-2009.

——, ——, M. Ponater, and C. Frömming, 2010: Importance of representing optical depth variability for estimates of global line-shaped contrail radiative forcing. *Proc. Natl. Acad. Sci. USA*, **107**, 19 181–19 184, https://doi.org/10.1073/pnas.1005555107.

——, ——, A. Bier, L. Bock, and I. J. Ford, 2015: The microphysical pathway to contrail formation. *J. Geophys. Res.*, **120**, 7893–7927, https://doi.org/10.1002/2015JD023491.

Klocke, D., J. Quaas, and B. Stevens, 2013: Assessment of different metrics for physical climate feedbacks. *Climate Dyn.*, **41**, 1173–1185, https://doi.org/10.1007/s00382-013-1757-1.

Lee, D. S., D. W. Fahey, P. M. Forster, P. J. Newton, R. C. N. Wit, L. L. Lim, B. Owen, and R. Sausen, 2009: Aviation and global climate change in the 21st century. *Atmos. Environ.*, **43**, 3520–3537, https://doi.org/10.1016/j.atmosenv.2009.04.024.

——, and Coauthors, 2010: Transport impacts on atmosphere and climate: Aviation. *Atmos. Environ.*, **44**, 4678–4734, https://doi.org/10.1016/j.atmosenv.2009.06.005.

Lohmann, U., P. Spichtinger, S. Heidt, T. Peter, and H. Smit, 2008: Cirrus clouds and ice supersaturation regions in a global climate model. *Environ. Res. Lett.*, **3**, 045022, https://doi.org/10.1088/1748-9326/3/4/045022.

——, and Coauthors, 2010: Total aerosol effect: Radiative forcing or radiative flux perturbation. *Atmos. Chem. Phys.*, **10**, 3235–3246, https://doi.org/10.5194/acp-10-3235-2010.

Manabe, S., and R. T. Wetherald, 1967: Thermal equilibrium of the atmosphere with a given distribution of relative humidity. *J. Atmos. Sci.*, **24**, 241–259, https://doi.org/10.1175/1520-0469(1967)024<0241:TEOTAW>2.0.CO;2.

Mannstein, H., P. Spichtinger, and K. Gierens, 2005: A note on how to avoid contrail cirrus. *Transport. Res.*, **10D**, 421–426, https://doi.org/10.1016/J.TRD.2005.04.012.

Marquart, S., M. Ponater, F. Mager, and R. Sausen, 2003: Future development of contrail cover, optical depth, and radiative forcing: Impacts of increasing air traffic and climate change. *J. Climate*, **16**, 2890–2904, https://doi.org/10.1175/1520-0442(2003)016<2890:FDOCCO>2.0.CO;2.

Marvel, K., G. A. Schmidt, R. L. Miller, and L. S. Nazarenko, 2016: Implications for climate sensitivity from the response to individual forcings. *Nat. Climate Change*, **6**, 386–389, https://doi.org/10.1038/nclimate2888.

Minnis, P., and Coauthors, 2013: Linear contrail and contrail cirrus properties determined from satellite data. *Geophys. Res. Lett.*, **40**, 3220–3226, https://doi.org/10.1002/grl.50569.

Myhre, G., and Coauthors, 2009: Intercomparison of radiative forcing calculations of stratospheric water vapour and contrails. *Meteor. Z.*, **18**, 585–596, https://doi.org/10.1127/0941-2948/2009/0411.

——, and Coauthors, 2013: Anthropogenic and natural radiative forcing. *Climate Change 2013: The Physical Science Basis.*, T. F. Stocker and Coauthors, Eds., Cambridge University Press, 659–740.

National Research Council, 2005: *Radiative Forcing of Climate Change*. National Academies Press, 207 pp.

Penner, J., D. H. Lister, D. J. Griggs, D. J. Dokken, and M. McFarland, Eds., 1999: Aviation and the *Global Atmosphere*. Cambridge University Press (special report for the IPCC), 373 pp.

——, C. Zhou, A. Garnier, and D. L. Mitchell, 2018: Anthropogenic aerosol indirect effects in cirrus clouds. *J. Geophys. Res.*, **123**, 11 652–11 677, https://doi.org/10.1029/2018JD029204.

Ponater, M., 2010: Distinctive efficacies of the components contributing to total aviation climate impact. *Proc. Second Int. Conf. on Transport, Atmosphere and Climate (TAC–2)*, Aachen, Germany, Deutsches Zentrum für Luft- und Raumfahrt, 227–232, https://elib.dlr.de/65284/.

——, S. Marquart, R. Sausen, and U. Schumann, 2005: On contrail climate sensitivity. *Geophys. Res. Lett.*, **32**, L10706, https://doi.org/10.1029/2005GL022580.

——, S. Pechtl, R. Sausen, U. Schumann, and G. Hüttig, 2006: Potential of the cryoplane technology to reduce aircraft climate impact: A state-of-the-art assessment. *Atmos. Environ.*, **40**, 6928–6944, https://doi.org/10.1016/j.atmosenv.2006.06.036.

Ramaswamy, V., and Coauthors, 2019: Radiative forcing of climate: The historical evolution of the radiative forcing concept, the forcing agents and their quantification, and applications. *A Century of Progress in Atmospheric and Related Sciences: Celebrating the American Meteorological Society Centennial, Meteor. Monogr.*, Vol. 59, 14.1–14.101, https://doi.org/10.1175/AMSMONOGRAPHS-D-19-0001.1.

Rap, A., P. M. Forster, J. M. Haywood, A. Jones, and O. Boucher, 2010: Estimating the climate impact of linear contrails using the UK Met Office climate model. *Geophys. Res. Lett.*, **37**, L20703, https://doi.org/10.1029/2010GL045161.

Rieger, V. S., S. Dietmüller, and M. Ponater, 2017: Can feedback analysis be used to uncover the physical origin of climate sensitivity and efficacy differences? *Climate Dyn.*, **49**, 2831–2844, https://doi.org/10.1007/s00382-016-3476-x.

Righi, M., J. Hendricks, and R. Sausen, 2016: The global impact of the transport sectors on atmospheric aerosol in 2030—Part 2: Aviation. *Atmos. Chem. Phys.*, **16**, 4481–4495, https://doi.org/10.5194/acp-16-4481-2016.

Roeckner, E., and Coauthors, 2004: The atmospheric general circulation model ECHAM5, Part 1, Model description. Tech. Rep. 349, Max-Planck Institut für Meteorologie, Hamburg, Germany, 127 pp.

——, and Coauthors, 2006: Sensitivity of simulated climate to horizontal and vertical resolution in the ECHAM5 atmosphere model. *J. Climate*, **19**, 3771–3791, https://doi.org/10.1175/JCLI3824.1.

Sausen, R., and Coauthors, 2005: Aviation radiative forcing in 2000: an update on IPCC (1999). *Meteor. Z.*, **14**, 555–561, https://doi.org/10.1127/0941-2948/2005/0049.

Schäfer, A. W., and I. A. Waitz, 2014: Air transportation and the environment. *Transp. Policy*, **34**, 1–4, https://doi.org/10.1016/j.tranpol.2014.02.012.

Schumann, U., and K. Graf, 2013: Aviation-induced cirrus and radiation changes at diurnal timescales. *J. Geophys. Res.*, **118**, 2404–2421, https://doi.org/10.1002/jgrd.50184.

——, and B. Mayer, 2017: Sensitivity of surface temperature to radiative forcing by contrail cirrus in a radiative-mixing model. *Atmos. Chem. Phys.*, **17**, 13 833–13 848, https://doi.org/10.5194/acp-17-13833-2017.

——, ——, K. Graf, and H. Mannstein, 2012: A parametric radiative forcing model for contrail cirrus. *J. Appl. Meteor. Climatol.*, **51**, 1391–1406, https://doi.org/10.1175/JAMC-D-11-0242.1.

——, J. E. Penner, Y. Chen, C. Zhou, and K. Graf, 2015: Dehydration effects from contrails in a coupled contrail-climate model. *Atmos. Chem. Phys.*, **15**, 11 179–11 199, https://doi.org/10.5194/acp-15-11179-2015.

Sherwood, S. C., S. Bony, O. Boucher, C. Bretherton, P. M. Forster, J. M. Gregory, and B. Stevens, 2015: Adjustments in the forcing-feedback framework for understanding climate change. *Bull. Amer. Meteor. Soc.*, **96**, 217–228, https://doi.org/10.1175/BAMS-D-13-00167.1.

Shindell, D. T., 2014: Inhomogeneous forcing and transient climate sensitivity. *Nat. Climate Change*, **4**, 274–277, https://doi.org/10.1038/nclimate2136.

Shine, K. P., J. Cook, E. Highwood, and M. Joshi, 2003: An alternative to radiative forcing for estimating the relative importance of climate change mechanisms. *Geophys. Res. Lett.*, **30**, 2047, https://doi.org/10.1029/2003GL018141.

——, E. J. Highwood, G. Rädel, N. Stuber, and Y. Balkanski, 2012: Climate model calculations of the impact of aerosols from road transport and shipping. *Atmos. Oceanic Opt.*, **25**, 62–70, https://doi.org/10.1134/S1024856012010125.

Smith, C. J., and Coauthors, 2018: Understanding rapid adjustments to diverse forcing agents. *Geophys. Res. Lett.*, **45**, 12 023–12 031, https://doi.org/10.1029/2018GL079826.

Soden, B., I. M. Held, R. Colman, K. M. Shell, J. T. Kiehl, and C. A. Shields, 2008: Quantifying climate feedbacks using radiative kernels. *J. Climate*, **21**, 3504–3520, https://doi.org/10.1175/2007JCLI2110.1.

Stevens, B., and Coauthors, 2013: Atmospheric component of the MPI-M Earth system model: ECHAM6. *J. Adv. Model. Earth Syst.*, **5**, 146–172, https://doi.org/10.1002/jame.20015.

Stuber, N., R. Sausen, and M. Ponater, 2001: Stratosphere adjusted radiative forcing calculations in a comprehensive climate model. *Theor. Appl. Climatol.*, **68**, 125–135, https://doi.org/10.1007/s007040170041.

Unterstrasser, S., K. Gierens, I. Sölch, and M. Lainer, 2017: Numerical simulations of homogeneously nucleated natural cirrus and contrail-cirrus. Part 1: How different are they? *Meteor. Z.*, **26**, 621–642, https://doi.org/10.1127/METZ/2016/0777.

Vázquez-Navarro, M., H. Mannstein, and S. Kox, 2015: Contrail life cycle and properties from 1 year of MSG/SEVIRI rapid-scan images. *Atmos. Chem. Phys.*, **15**, 8739–8749, https://doi.org/10.5194/acp-15-8739-2015.

Vial, J., J.-L. Dufresne, and S. Bony, 2013: On the interpretation of inter-model spread in CMIP5 climate sensitivity estimates. *Climate Dyn.*, **41**, 3339–3362, https://doi.org/10.1007/s00382-013-1725-9.

Webb, M. J., and Coauthors, 2017: The Cloud Feedback Model Intercomparison Project (CFMIP) contribution to CMIP6. *Geosci. Model Dev.*, **10**, 359–384, https://doi.org/10.5194/gmd-10-359-2017.

Wilkerson, J., M. Z. Jacobson, A. Malwitz, S. Balasubramanian, R. Wayson, G. Fleming, A. D. Naiman, and S. K. Lele, 2010: Analysis of emission data from global commercial aviation: 2004 and 2006. *Atmos. Chem. Phys.*, **10**, 6391–6408, https://doi.org/10.5194/acp-10-6391-2010.

Yoshimori, M., and S. Broccoli, 2008: Equilibrium response of an atmosphere–mixed layer ocean model to different radiative forcing agents: Global and zonal mean response. *J. Climate*, **21**, 4399–4423, https://doi.org/10.1175/2008JCLI2172.1.

Zelinka, M. D., S. A. Klein, and D. L. Hartmann, 2012: Computing and partitioning cloud feedbacks using cloud property histograms. Part I: Cloud radiative kernels. *J. Climate*, **25**, 3715–3735, https://doi.org/10.1175/JCLI-D-11-00248.1.

——, ——, K. E. Taylor, T. Andrews, M. J. Webb, J. M. Gregory, and P. M. Forster, 2013: Contributions of different cloud types to feedbacks and rapid adjustments in CMIP5. *J. Climate*, **26**, 5007–5027, https://doi.org/10.1175/JCLI-D-12-00555.1.

Zhou, C., and J. E. Penner, 2014: Aircraft soot indirect effect on large-scale cirrus clouds: Is the indirect forcing by aircraft soot positive or negative? *J. Geophys. Res. Atmos.*, **119**, 11 303–11 320, https://doi.org/10.1002/2014JD021914.